A Novel Control Strategy for a Variable-Speed Wind Turbine With a Permanent-Magnet Synchronous Generator

Md. Enamul Haque, *Member, IEEE*, Michael Negnevitsky, *Senior Member, IEEE*, and Kashem M. Muttaqi, *Senior Member, IEEE*

***Abstract*—This paper presents a novel control strategy for the operation of a direct-drive permanent-magnet synchronous-generator-based stand-alone variable-speed wind turbine. The control strategy for the generator-side converter with maximum power extraction is presented. The stand-alone control is featured with output voltage and frequency controller that is capable of handling variable load. The potential excess of power is dissipated in the dump-load resistor with the chopper control, and the dc-link voltage is maintained. Dynamic representation of dc bus and small-signal analysis are presented. Simulation results show that the controllers can extract maximum power and regulate the voltage and frequency under varying wind and load conditions. The controller shows very good dynamic and steady-state performance.**

***Index Terms*—Maximum power extraction, permanent-magnet synchronous generator (PMSG), switch-mode rectifier, variable-speed wind turbine, voltage and frequency control.**

I. Introduction

VARIABLE-SPEED wind turbines have many advantages over fixed-speed generation such as increased energy capture, operation at maximum power point, improved efficiency, and power quality [1]. However, the presence of a gearbox that couples the wind turbine to the generator causes problems. The gearbox suffers from faults and requires regular maintenance [2]. The reliability of the variable-speed wind turbine can be improved significantly by using a direct-drive permanent-magnet synchronous generator (PMSG). PMSG has received much attention in wind-energy application because of their property of self-excitation, which allows an operation at a high power factor and high efficiency [3]. The use of permanent magnet in the rotor of the PMSG makes it unnecessary to supply magnetizing current through the stator for constant air-gap flux; the stator current need only to be torque producing. Hence, for the same output, the PMSG will operate at a higher power factor because of the absence of the magnetizing current and will be more efficient than other machines.

To extract maximum power from the fluctuating wind, variable-speed operation of the wind-turbine generator is necessary. This requires a sophisticated control strategy for the generator. Optimum power/torque tracking is a popular control strategy, as it helps to achieve optimum wind-energy utilization [4]–[8]. Some of these control strategies use wind velocity to obtain the desired shaft speed to vary the generator speed. However, anemometer-based control strategy increases cost and reduces the reliability of the overall system. These control strategies are not suitable or too expensive for a small-scale wind turbine. In [7], the current vector of an interior-type PMSG is controlled to optimize the wind-turbine operation at various wind speed, which requires six active switches to be controlled. Switch-mode rectifier has been investigated for use with automotive alternator with permanent-magnet synchronous machines [9], [10]. The switch-mode rectifier has also been investigated for small-scale variable-speed wind turbine [11], [12].

A control strategy for the generator-side converter with output maximization of a PMSG-based small-scale wind turbine is developed. The generator-side switch-mode rectifier is controlled to achieve maximum power from the wind. The method requires only one active switching device [insulated-gate bipolar transistor (IGBT)], which is used to control the generator torque to extract maximum power. It is simple and a low-cost solution for a small-scale wind turbine.

For a stand-alone system, the output voltage of the load-side converter has to be controlled in terms of amplitude and frequency. Previous publications related to PMSG-based variable-speed wind turbine are mostly concentrated on grid-connected system [6]–[8]. Much attention has not been paid for a stand-alone system. Many countries are affluent in renewable-energy resources; however, they are located in remote areas where power grid is not available. Local small-scale stand-alone distributed generation system can utilize these renewable-energy resources when grid connection is not feasible. In this paper, a control strategy is developed to control the load voltage in a stand-alone mode. As there is no grid in a stand-alone

Paper ICPSD-09-047, presented at the 2008 Industry Applications Society Annual Meeting, Edmonton, AB, Canada, October 5–9, and approved for publication in the IEEE Transactions on Industry Applications by the Power Systems Engineering Committee of the IEEE Industry Applications Society. Manuscript submitted for review November 30, 2008 and released for publication June 24, 2009. First published November 20, 2009; current version published January 20, 2010. This work was supported in part by the Australian Research Council and in part by Hydro Tasmania Linkage Grant K0015166.

M. E. Haque and M. Negnevitsky are with the School of Engineering, University of Tasmania, Hobart, TAS 7001, Australia (e-mail: mehaque@utas.edu.au).

K. M. Muttaqi is with the School of Electrical, Computer and Telecommunication Engineering, University of Wollongong, Wollongong, NSW 2522, Australia (e-mail: kashem@uow.edu.au).

Color versions of one or more of the figures in this paper are available online at http://ieeexplore.ieee.org.

Digital Object Identifier 10.1109/TIA.2009.2036550

system, the output voltage has to be controlled in terms of amplitude and frequency. The load-side pulsewidth modulation (PWM) inverter is using a relatively complex vector-control scheme to control the amplitude and frequency of the inverter output voltage. The stand-alone control is featured with output voltage and frequency controller capable of handling variable load. A dump-load-resistor controller is used to dissipate excess power during fault or over generation. The excess power is dissipated in the dump-load resistor with the chopper control, and the dc-link voltage is maintained.

II. Wind-Turbine Characteristics

The amount of power captured by the wind turbine (power delivered by the rotor) is given by

$$P_t = 0.5\rho A C_p(\lambda,\beta)\times(v_w)^3 = 0.5\rho A C_p \times \left(\frac{\omega_m R}{\lambda}\right)^3 \quad (1)$$

where ρ is the air density (kilograms per cubic meter), v_ω is the wind speed in meters per second, A is the blades' swept area, and C_p is the turbine-rotor-power coefficient, which is a function of the tip-speed ratio (λ) and pitch angle (β). $\omega_m =$ rotational speed of turbine rotor in mechanical radians per second, and $R =$ radius of the turbine. The coefficient of performance of a wind turbine is influenced by the tip-speed to wind-speed ratio, which is given by

$$\text{TSR} = \lambda = \frac{\omega_m R}{v_w}. \quad (2)$$

The wind turbine can produce maximum power when the turbine operates at maximum C_p (i.e., at C_{p_opt}). Therefore, it is necessary to keep the rotor speed at an optimum value of the tip-speed ratio λ_{opt}. If the wind speed varies, the rotor speed should be adjusted to follow the change.

The target optimum power from a wind turbine can be written as

$$P_{m\_\text{opt}} = 0.5\rho A C_{p\_\text{opt}} \left(\omega_{\frac{m\_\text{opt}R}{\lambda_{\text{opt}}}}\right)^3 = K_{\text{opt}}\left(\omega_{m\_\text{opt}}\right)^3 \quad (3)$$

where

$$K_{\text{opt}} = 0.5\rho A C_{p\_\text{opt}} \left(\frac{R}{\lambda_{\text{opt}}}\right)^3 \quad (4)$$

$$\omega_{m\_\text{opt}} = \frac{\lambda_{\text{opt}}}{R} v_w = K_w v_w. \quad (5)$$

Therefore, the target optimum torque can be given by

$$T_{m\_\text{opt}} = K_{\text{opt}}\left(\omega_{m\_\text{opt}}\right)^2. \quad (6)$$

The mechanical rotor power generated by the turbine as a function of the rotor speed for different wind speed is shown in Fig. 1. The optimum power is also shown in this figure. The optimum power curve (P_{opt}) shows how maximum energy can be captured from the fluctuating wind. The function of the controller is to keep the turbine operating on this curve, as the wind velocity varies. It is observed from this figure that there is always a matching rotor speed which produces optimum power

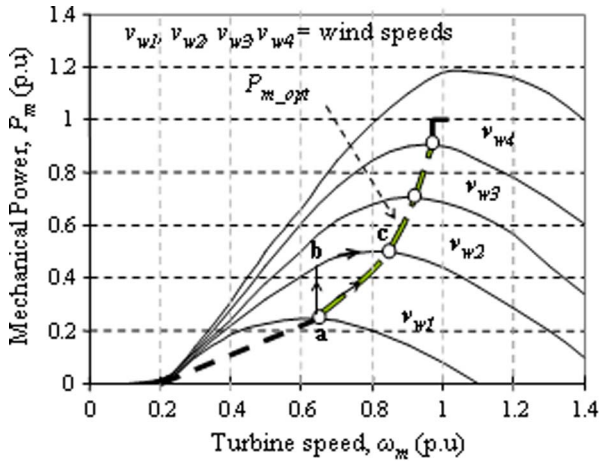

Fig. 1. Mechanical power generated by the turbine as a function of the rotor speed for different wind speeds.

for any wind speed. If the controller can properly follow the optimum curve, the wind turbine will produce maximum power at any speed within the allowable range. The optimum torque can be calculated from the optimum power given by (6). For the generator speed below the rated maximum speed, the generator follows (6).

III. System Overview

Fig. 2 shows the control structure of a PMSG-based stand-alone variable-speed wind turbine which include a wind turbine, PMSG, single-switch three-phase switch-mode rectifier, and a vector-controlled PWM voltage-source inverter.

The output of a variable-speed PMSG is not suitable for use as it varies in amplitude and frequency due to fluctuating wind. A constant dc voltage is required for direct use, storage, or conversion to ac via an inverter. In this paper, a single-switch three-phase switch-mode rectifier is used to convert the ac output voltage of the generator to a constant dc voltage before conversion to ac voltage via an inverter.

The single-switch three-phase switch-mode rectifier consists of a three-phase diode bridge rectifier and a dc to dc converter. The output of the switch-mode rectifier can be controlled by controlling the duty cycle of an active switch (such as IGBT) at any wind speed to extract maximum power from the wind turbine and to supply the loads. A vector-controlled IGBT inverter is used to regulate the output voltage and frequency during load or wind variations. Voltage drop due to sudden fall in wind speed can be compensated by the energy-storage system. During wind gust, the dump-load controller will be activated to regulate the dc-link voltage to maintain the output load voltage at the desired value.

IV. Control of Switch-Mode Rectifier With Maximum Power Extraction

The structure of the proposed control strategy of the switch-mode rectifier is shown in Fig. 3. The control objective is to control the duty cycle of the switch $\boldsymbol{S}$ in Fig. 2 to extract maximum power from the variable-speed wind turbine and

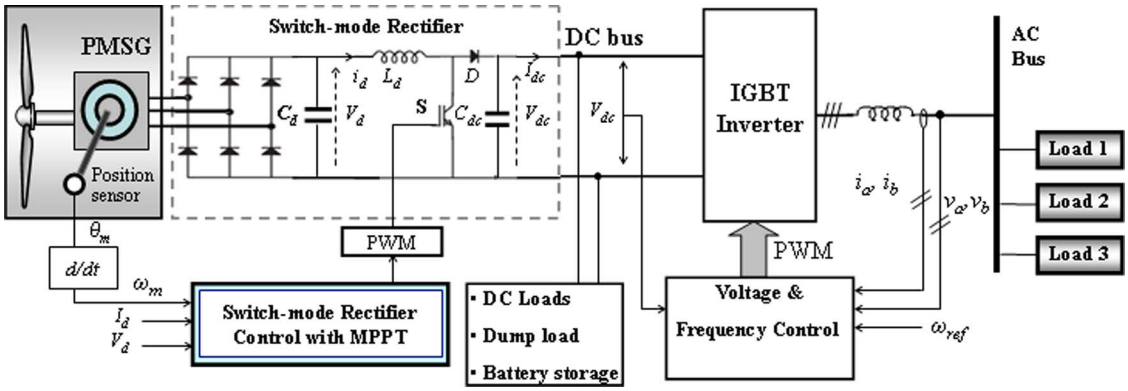

Fig. 2. Control structure of a PMSG-based stand-alone variable-speed wind turbine.

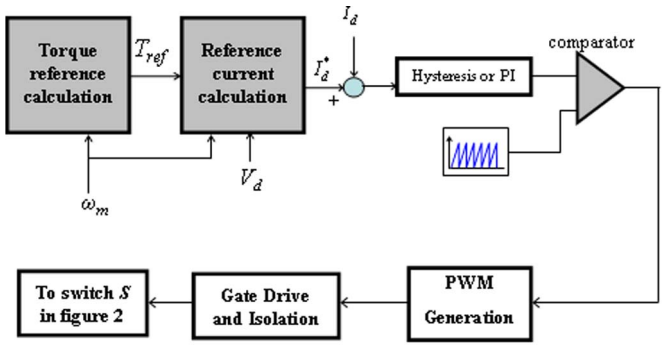

Fig. 3. Control strategy of the switch-mode rectifier.

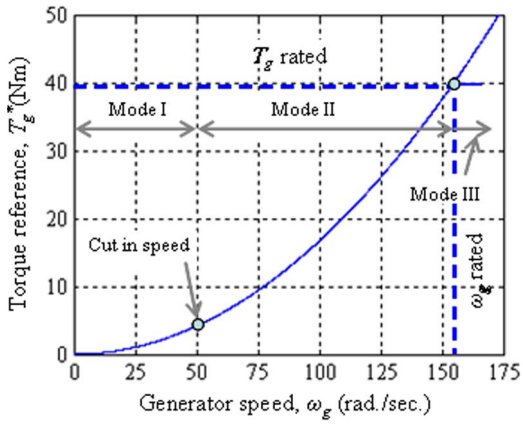

Fig. 4. Generator torque reference versus speed.

transfer the power to the load. The control algorithm includes the following steps.

1) Measure generator speed ω_g.
2) Determine the reference torque (Fig. 4) using the following equation:

$$T_g^* = K_{\text{opt}}(\omega_g)^2. \tag{7}$$

3) This torque reference is then used to calculate the dc current reference by measuring the rectifier output voltage V_d as given by

$$I_d^* = \left(T_g^* \times \omega_g\right)/V_d. \tag{8}$$

4) The error between the reference dc current and measured dc current is used to vary the duty cycle of the switch to regulate the output of the switch-mode rectifier and the generator torque through a proportional–integral (PI) controller.

The generator torque is controlled in the optimum torque curve as shown in Fig. 4 according to the generator speed. The acceleration or deceleration of the generator is determined by the difference of the turbine torque T_m and generator torque T_g. If the generator speed is less than the optimal speed, the turbine torque is larger than the generator torque, and the generator will be accelerated. The generator will be decelerated if the generator speed is higher than the optimal speed. Therefore, the turbine and generator torques settle down to the optimum torque point T_{m_opt} at any wind speed, and the wind turbine is operated at the maximum power point. For example (considering Fig. 1), if the PMSG is operating at point "**a**" and the wind speed increases from v_{w1} to v_{w2} (point "**b**"), the additional power and, hence, torque causes the PMSG to accelerate. The accelerating torque is the difference between the turbine mechanical torque and the torque given by the optimum curve. Finally, the generator will reach the point " **c**" where the accelerating torque is zero. A similar situation occurs when the wind velocity decreases.

In the proposed method, the wind speed is not required to be monitored, and, therefore, it is a simple output-maximization control method without wind-speed sensor (anemometer).

V. Control of Load-Side Inverter

The objective of the supply-side converter is to regulate the voltage and frequency. The output voltages have to be controlled in terms of amplitude and frequency as no grid exists in a stand-alone system. The control structure for stand-alone control mode consists of output-voltage controller, dc-link voltage controller, dump-load-resistance controller, and current controller. The output-voltage controller is used to control the output voltage during load transients or wind variation. The dc-link voltage controller is used to stabilize the dc-link voltage. The dc voltage PI controller maintains the dc voltage to the reference value. The PI controllers are used to regulate the output voltage and currents in the inner control loops and the dc voltage controller in the outer loop. To compensate

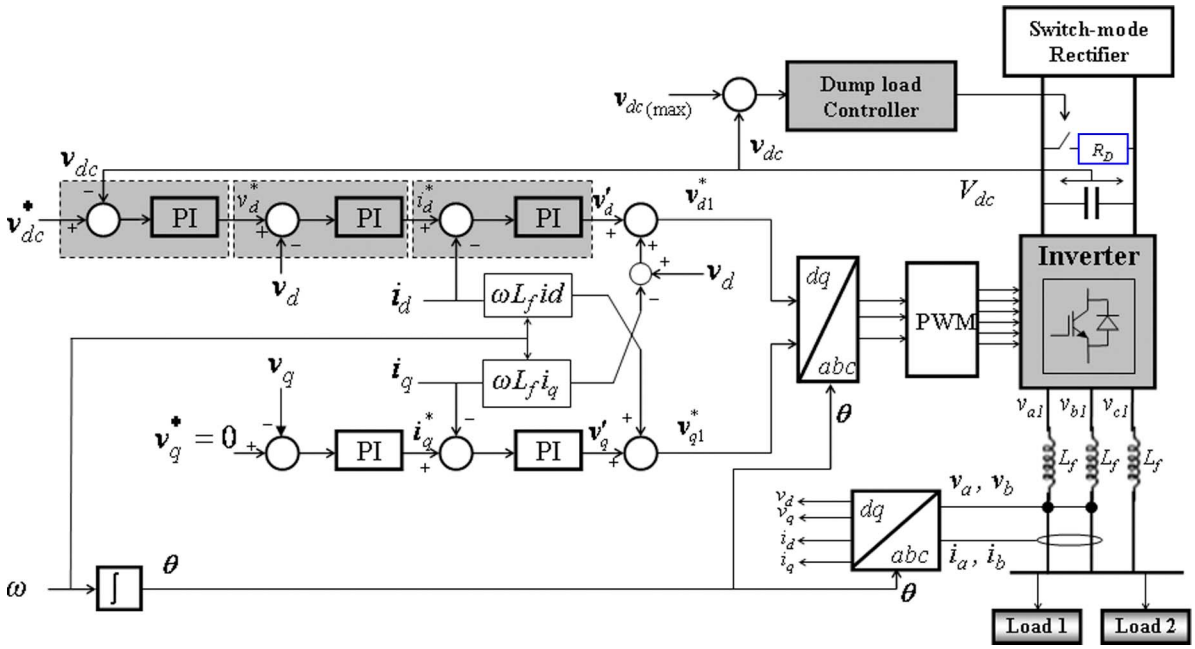

Fig. 5. Vector-control structure for stand-alone mode of operation.

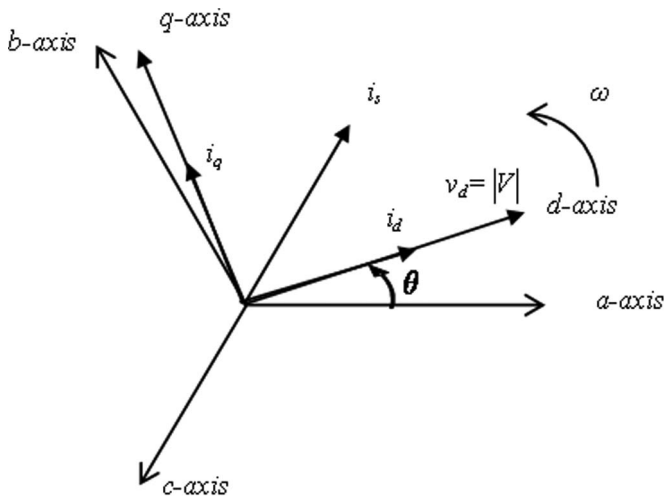

Fig. 6. abc and the rotating reference frame.

for the cross-coupling effect due to the output filter in the rotating reference frame, compensation terms are added as shown in Fig. 5. All the PI controllers are tuned using the Ziegler–Nichols tuning method [13].

The vector-control scheme used is based on a synchronously rotating reference frame as shown in Fig. 6. The angular velocity of the rotating axis system ω is set in the controller and defines the electrical frequency at the load. The voltage balance across the inductor L_f is given by

$$\begin{bmatrix} v_a \\ v_b \\ v_c \end{bmatrix} = R_f \begin{bmatrix} i_a \\ i_b \\ i_c \end{bmatrix} + L_f \frac{d}{dt} \begin{bmatrix} i_a \\ i_b \\ i_c \end{bmatrix} + \begin{bmatrix} v_{a1} \\ v_{b1} \\ v_{c1} \end{bmatrix} \tag{9}$$

where L_f and R_f are the filter inductance and resistance, respectively. v_{a1}, v_{b1}, and v_{c1} represent the voltages at the inverter output. i_a, i_b, and i_c are the line currents.

The vector representation of a balanced three-phase system and their equivalent vectors in a rotating dq reference frame is shown in Fig. 6. Transforming the voltage equations using dq transformation in the rotating reference frame

$$v_d = v_{d1} - R_f i_d - L_f \frac{di_d}{dt} + \omega L_f i_q \tag{10}$$

$$v_q = v_{q1} - R_f i_q - L_f \frac{di_q}{dt} - \omega L_f i_d. \tag{11}$$

The instantaneous power in a three-phase system is given by

$$P(t) = v_a i_a + v_b i_b + v_c i_c = [v_a \quad v_b \quad v_c]\,[i_a \quad i_b \quad i_c]^{'}. \tag{12}$$

Using dq transformation, the active and reactive power is given by

$$P = \frac{3}{2}\left(v_d i_d + v_q i_q\right) \tag{13}$$

$$Q = \frac{3}{2}\left(v_d i_q + v_q i_d\right). \tag{14}$$

If the reference frame is as $v_q = 0$ and $v_d = |V|$, the equations for the active and reactive power will be

$$P = \frac{3}{2}(v_d i_d) = \frac{3}{2}|V| i_d \tag{15}$$

$$Q = \frac{3}{2}(v_d i_q) = \frac{3}{2}|V| i_q. \tag{16}$$

Therefore, the active and reactive power can be controlled by controlling the direct and quadrature current components, respectively.

VI. DC-Bus Dynamics and Protection

A dump-resistor controller is used to dissipate excess power during fault or overgeneration. The potential excess of power

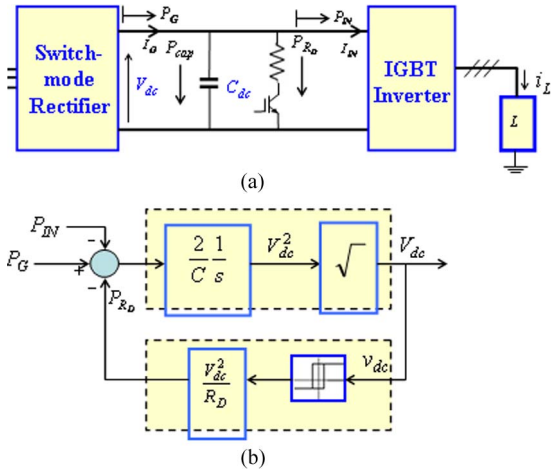

Fig. 7. Dynamic representation of a dc bus and protection. (a) Power flow in the dc link. (b) DC-bus dynamics and protection.

will be dissipated in the dump-load resistor with the chopper control, and the dc-link voltage will be maintained. The control is linear and increases the duty cycle as a function of the overvoltage amount. If the dc-link voltage exceeds the maximum limit, the dc link will be short-circuited through the resistor R_D as shown in Fig. 7. Using the power-balance principle, the dynamic behavior of the dc-bus voltage $V_{\rm dc}$ is given by

$$\frac{d\left(\frac{1}{2}CV_{\rm dc}^2\right)}{dt} = P_G - \frac{V_{\rm dc}^2}{R_D} - P_{\rm IN} \tag{17}$$

$$\Rightarrow \frac{d(V_{dc}^2)}{dt} = \frac{2}{C} \times \left(P_G - \frac{V_{\rm dc}^2}{R_D} - P_{\rm IN}\right)$$

$$\Rightarrow V_{\rm dc} = \sqrt{\frac{2}{C}\int \left(P_G - \frac{V_{\rm dc}^2}{R_D} - P_{\rm IN}\right) dt} \tag{18}$$

where $P_G =$ Power from the generator, $(V_{\rm dc}^2/R_D) =$ power dissipated in the dump-load resistor (R_D), and $P_{\rm IN} =$ power at the input of the inverter.

VII. Small-Signal Analysis

Considering that the load power factor is close to unity, the reactive power supplied by the converter will be negligible. Therefore, the quadrature component of the load current will be zero. For an R_L load, the $d-q$ equations for the load side of Fig. 7(a) are

$$I_{\rm IN} \approx \frac{v_d i_{dL}}{V_{dc}} \tag{19}$$

$$v_d = i_{dL} R_L \tag{20}$$

where v_d and i_{dL} are the direct component of the load voltage and current, respectively.

The dc-link voltage $V_{\rm dc}$ is given by

$$V_{\rm dc} = \frac{I_G - I_{\rm IN}}{sC_{\rm dc}} \tag{21}$$

where $C_{\rm dc}$ is the dc-link capacitance. Using (19)–(21), the block diagram of Fig. 8(a) can be obtained. In Fig. 8(a), $G_{\rm dc}(s)$

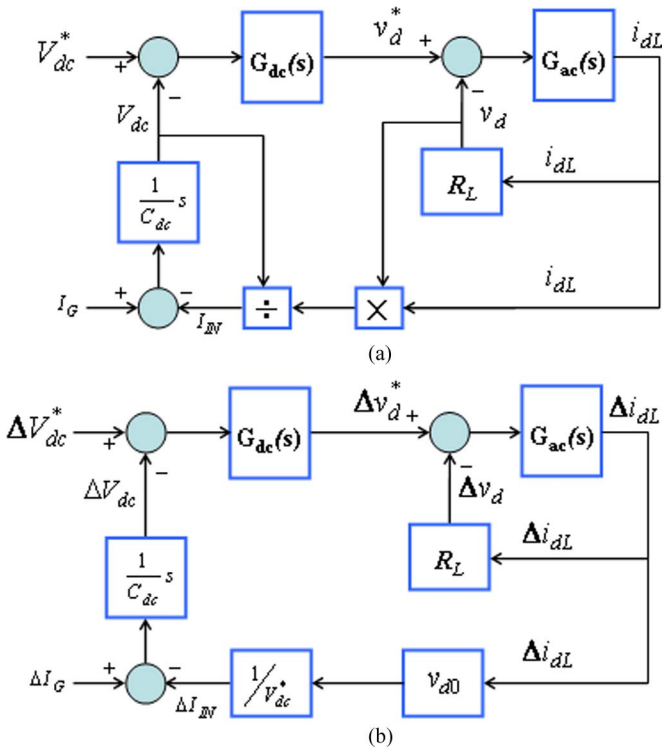

Fig. 8. Block diagram of the proposed control system. (a) Control system. (b) Small-signal model.

is the dc-link voltage controller, as shown in Fig. 5, and $G_{\rm ac}(s)$ is the controller of the ac load voltage. The control system of Fig. 8(a) is nonlinear with a coupling between the dc-link voltage control loop and load voltage control loop. Linearizing around a quiescent point $(V_{\rm dc0}, v_{d0}, i_{dL0}, I_{G0}, I_{\rm IN0})$ gives

$$\Delta I_{\rm IN} = \frac{\Delta v_d i_{dL0} + \Delta i_{dL} v_{d0}}{V_{\rm dc0}} - \frac{v_{d0} i_{dL0}}{V_{\rm dc0}^2}\Delta V_{\rm dc} \tag{22}$$

$$\Delta V_{\rm dc} = \frac{\Delta I_G - \Delta I_{\rm IN}}{sC_{\rm dc}}. \tag{23}$$

Under normal operation, the small-signal model can be simplified by considering that the variation in the dc-link voltage and direct-axis component of the load voltage is small compared with the variation in load currents. Therefore

$$\frac{v_{d0}}{V_{\rm dc0}}\Delta i_{dL} \gg \frac{i_{dL0}}{V_{\rm dc0}}\Delta v_d - \frac{v_{d0} i_{dG0}}{V_{\rm dc0}^2}\Delta V_{\rm dc}. \tag{24}$$

Using (22)–(24), the small-signal model of Fig. 8(b) is obtained. There is still some coupling between the dc-link voltage and the load-voltage control loops in Fig. 8(b). However, because of the high inertia of the wind turbine [14], the current will vary slowly compared with the natural frequency of the load-voltage control loop. Therefore, the load voltage can be considered almost constant for the dc-link voltage control loop, and the open-loop transfer function $\Delta V_{\rm dc}/\Delta i_{dL}$ is obtained as

$$\frac{\Delta V_{\rm dc}}{\Delta i_{dL}} \approx \frac{v_{d0}}{sC_{\rm dc}V_{\rm dc}^*}. \tag{25}$$

TABLE I
PARAMETERS OF TURBINE-GENERATOR SYSTEM

Wind turbine	
Density of air	1.225 Kg/m^3
Area swept by blades, A	1.06 m^2
Optimum coefficient, K_{opt}	1.67×10^{-3} Nm/(rad/s)^2
Base wind speed	12 m/s
PMSG	
No. of poles	10
Rated speed	153 rad/sec
Rated current	12 A
Armature resistance, R_s	0.425 Ω
Magnet flux linkage	0.433 Wb
Stator inductance, L_s	8.4 mH
Rated torque	40 Nm
Rated power	6 KW

A PI controller can be designed using (25). The open-loop transfer function for the load-voltage control loop can also be obtained from Fig. 8(b) as

$$\frac{\Delta v_d}{\Delta i_{dL}} \approx R_L. \tag{26}$$

Considering the output filter capacitance (C_f) and neglecting the cross coupling between the d and q axes, the open-loop transfer function $\Delta v_d/\Delta i_{dL}$ is given by

$$\frac{\Delta v_d}{\Delta i_{dL}} \approx \frac{R_L}{1+sR_LC_f}. \tag{27}$$

Using (27), a PI controller for load-voltage control loop can be designed. The transfer function of (27) is obtained considering a resistive load. For an $R_L - L$ load, the transfer function of the filter capacitance and the load can be obtained (neglecting cross-coupling terms) as

$$\begin{bmatrix} v_d \\ v_q \end{bmatrix} \approx \frac{(s+R_L/L)}{C_f\left(s^2+(R_L/L)s+1/(LC_f)\right)} \begin{bmatrix} i_{dL} \\ i_{qL} \end{bmatrix} \tag{28}$$

where v_d and v_q are the $d-q$ axes components of the load voltage.

VIII. RESULTS AND DISCUSSION

The model of the PMSG-based variable-speed wind-turbine system of Fig. 2 is built using Matlab/Simpower dynamic system simulation software. The simulation model is developed based on a Kollmorgen 6-kW industrial permanent-magnet synchronous machine. The parameters of the turbine and PMSG used are given in Table I. The power converter and the control algorithm are also implemented and included in the model. The sampling time used for the simulation is 20 μs.

Fig. 9 shows the response of the system for a step change of wind speed from 10 to 12 to 9 m/s, and then back to 10 m/s. It is seen from Fig. 9(c) that the generated torque reference follows the optimum mechanical torque of the turbine quite well. The generator electromagnetic torque also track the reference torque as shown in Fig. 9(d).

Fig. 9(e) shows the reference dc current and measured dc current. It is observed that the measured dc current follows the reference dc current and regulate the turbine torque to extract

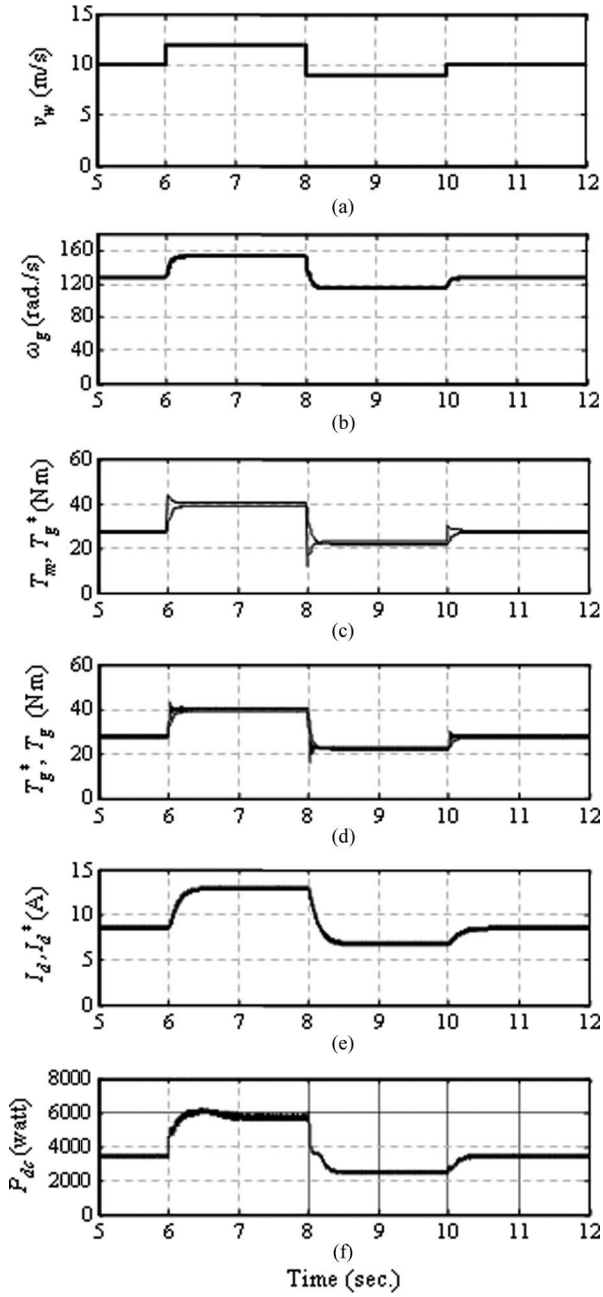

Fig. 9. Response of the system for a step change of wind speed from 10 to 12 to 9 to 10 m/s. (a) Wind speed. (b) Generator speed. (c) Turbine torque and torque reference. (d) Torque reference and generator electromagnetic torque. (e) DC current reference and dc current. (f) DC power output.

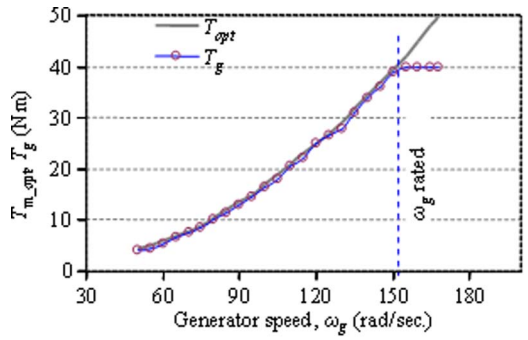

Fig. 10. Optimum torque and generator torque.

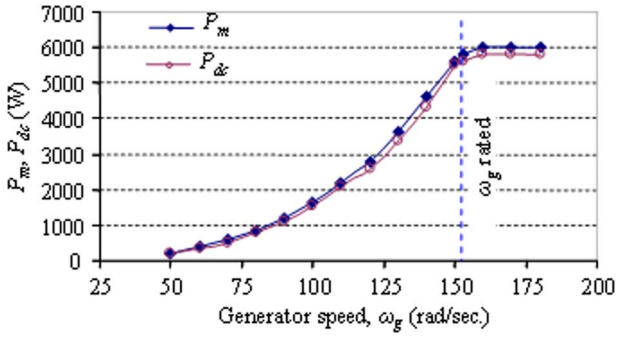

Fig. 11. Turbine mechanical input power and electrical output power.

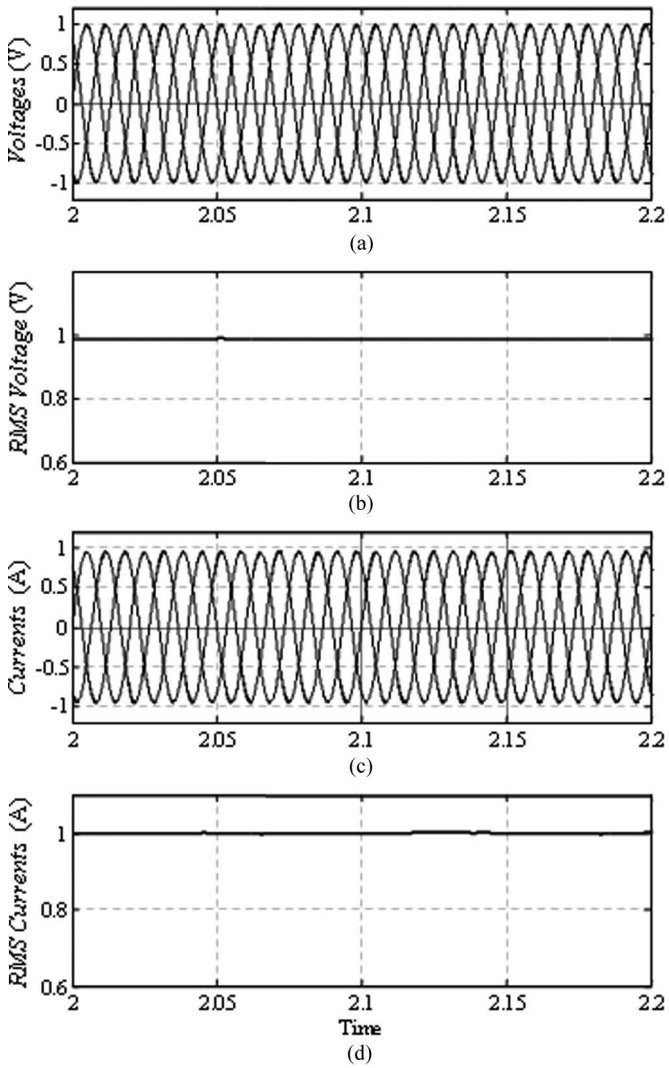

Fig. 12. Instantaneous and rms voltage and currents at a constant load (full load). (a) Instantaneous load voltages. (b) RMS line voltage. (c) Instantaneous line currents. (d) RMS line current.

maximum power from the wind turbine. Fig. 9(f) shows the dc output power.

Fig. 10 shows optimum torque versus speed as well as generator torque versus speed. The turbine mechanical input power and electrical output powers are shown in Fig. 11. It is observed that the torque and power follow the optimum curves up to the rated speed and extract maximum power.

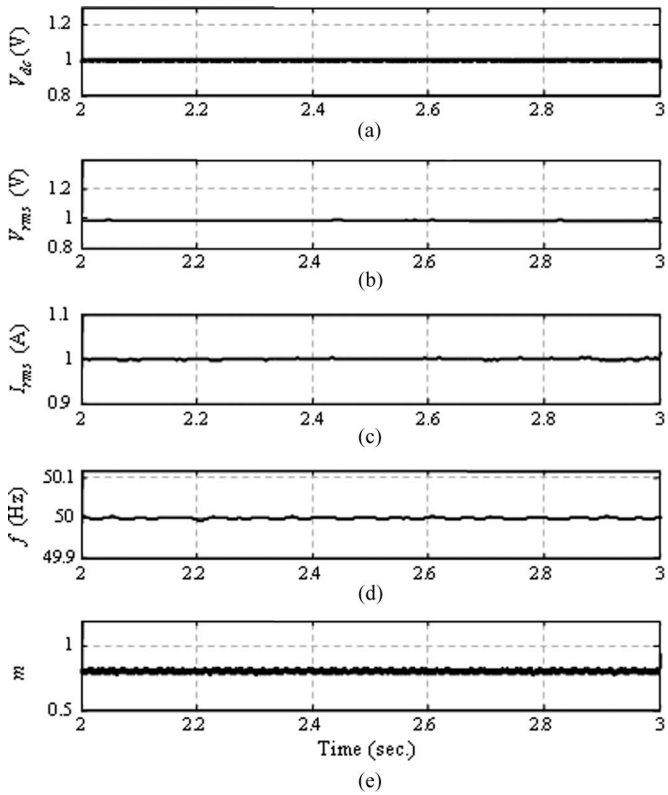

Fig. 13. DC-link voltage, rms load voltage, rms line current, frequency, and modulation index at a constant load (full load). (a) DC-link voltage. (b) RMS load voltage (L–L). (c) RMS load current. (d) Frequency. (e) Modulation index.

The simulation results demonstrate that the controller works very well and shows very good dynamic and steady-state performance. The control algorithm can be used to extract maximum power from the variable-speed wind turbine under fluctuating wind.

Fig. 12 shows the load voltage and current responses at a constant load. Fig. 12(a) and (b) shows the instantaneous and rms load voltages, and Fig. 12(c) and (d) shows the instantaneous and rms currents at a constant load. Fig. 13 shows the dc-link voltage, rms load voltage, rms line current, frequency response, and modulation index of the PWM inverter at a constant load. It is seen from Fig. 13(b) and (d) that the load voltage and frequency are well maintained at a constant-load condition.

Fig. 14 shows the instantaneous and rms load voltages and currents when the load changes from 100% to 50% and then from 50% to 100%. Fig. 14(a) and (b) shows the instantaneous and rms voltages, and Fig. 14(c) and (d) shows the instantaneous and rms currents when the load is reduced to 50% at $t = 3$ s and remains at this value until $t = 4$ s. It is observed that the voltage is well maintained despite the variation of loads. The load current is changing with the load variations as expected.

Fig. 15 shows the responses of the dc-link voltage, rms load voltage, rms line current, frequency, and modulation index of the PWM inverter under varying load condition. The load is reduced to 50% during $3\text{ s} \leq t \leq 4$ s.

It is seen that the controller can regulate the load voltage and frequency quite well at constant load and under varying load conditions.

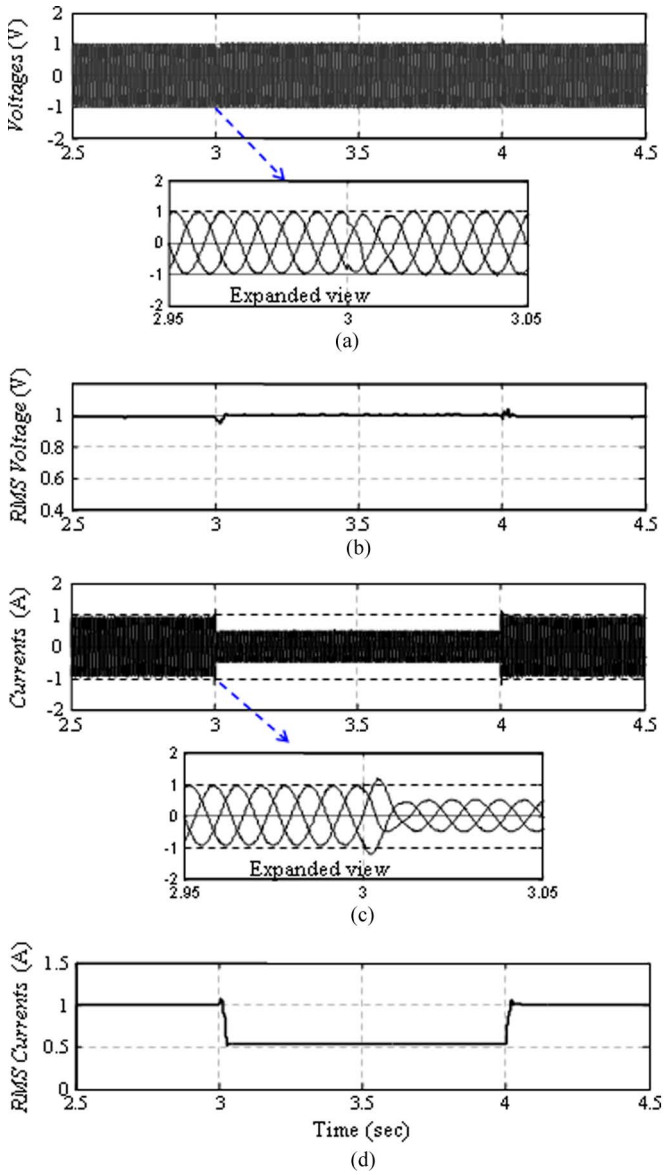

Fig. 14. Instantaneous and rms voltage and current responses when the load changes from 100% to 50% and from 50% to 100%. (a) Instantaneous load voltages. (b) RMS line voltage. (c) Instantaneous line currents. (d) RMS line current.

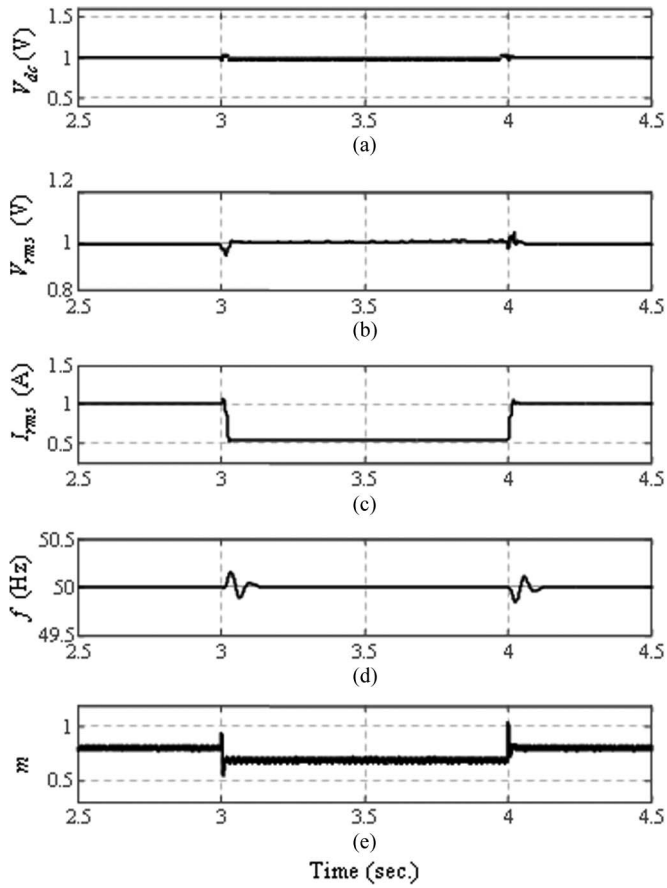

Fig. 15. Response of dc-link voltage, rms load voltage, rms line current, frequency, and modulation index when the load changes from 100% to 50% and from 50% to 100%. (a) DC-link voltage. (b) RMS load voltage (L–L). (c) RMS load current. (d) Frequency. (e) Modulation index.

IX. Conclusion

A control strategy for a direct-drive stand-alone variable-speed wind turbine with a PMSG has been presented in this paper. A simple control strategy for the generator-side converter to extract maximum power is discussed and implemented using Simpower dynamic-system simulation software. The controller is capable of maximizing output of the variable-speed wind turbine under fluctuating wind. The load-side PWM inverter is controlled using vector-control scheme to maintain the amplitude and frequency of the inverter output voltage. It is seen that the controller can maintain the load voltage and frequency quite well at constant load and under varying load condition. The generating system with the proposed control strategy is suitable for a small-scale stand-alone variable-speed wind-turbine installation for remote-area power supply. The simulation results demonstrate that the controller works very well and shows very good dynamic and steady-state performance.

Acknowledgment

The authors would like to thank the Hydro Tasmania personnel for their support and cooperation in providing information and advice on the operation of a remote-area power-supply system.

References

[1] S. Müller, M. Deicke, and R. W. De Doncker, "Doubly fed induction generator system for wind turbines," *IEEE Ind. Appl. Mag.*, vol. 8, no. 3, pp. 26–33, May 2002.
[2] H. Polinder, F. F. A. Van der Pijl, G. J. de Vilder, and P. J. Tavner, "Comparison of direct-drive and geared generator concepts for wind turbines," *IEEE Trans. Energy Convers.*, vol. 3, no. 21, pp. 725–733, Sep. 2006.
[3] T. F. Chan and L. L. Lai, "Permanent-magnet machines for distributed generation: A review," in *Proc. IEEE Power Eng. Annu. Meeting*, 2007, pp. 1–6.
[4] M. De Broe, S. Drouilhet, and V. Gevorgian, "A peak power tracker for small wind turbines in battery charging applications," *IEEE Trans. Energy Convers.*, vol. 14, no. 4, pp. 1630–1635, Dec. 1999.
[5] R. Datta and V. T. Ranganathan, "A method of tracking the peak power points for a variable speed wind energy conversion system," *IEEE Trans. Energy Convers.*, vol. 18, no. 1, pp. 163–168, Mar. 1999.
[6] K. Tan and S. Islam, "Optimal control strategies in energy conversion of PMSG wind turbine system without mechanical sensors," *IEEE Trans. Energy Convers.*, vol. 19, no. 2, pp. 392–399, Jun. 2004.

[7] S. Morimoto, H. Nakayama, M. Sanada, and Y. Takeda, "Sensorless output maximization control for variable-speed wind generation system using IPMSG," *IEEE Trans. Ind. Appl.*, vol. 41, no. 1, pp. 60–67, Jan. 2005.
[8] M. Chinchilla, S. Arnaltes, and J. C. Burgos, "Control of permanent-magnet generators applied to variable-speed wind-energy systems connected to the grid," *IEEE Trans. Energy Convers.*, vol. 21, no. 1, pp. 130–135, Mar. 2006.
[9] D. J. Perreault and V. Caliskan, "Automotive power generation and control," *IEEE Trans. Power Electron.*, vol. 19, no. 3, pp. 618–630, May 2004.
[10] W. L. Soong and N. Ertugrul, "Inverterless high-power interior permanent-magnet automotive alternator," in *IEEE Trans. Ind. Appl.*, Jul. 2004, vol. 40, no. 4, pp. 1083–1091.
[11] D. M. Whaley, W. L. Soong, and N. Ertugrul, "Investigation of switched-mode rectifier for control of small-scale wind turbines," in *Conf. Rec. IEEE IAS Annu. Meeting*, 2005, pp. 2849–2856.
[12] E. Muljadi, S. Drouilhet, R. Holz, and V. Gevorgian, "Analysis of permanent magnet generator for wind power battery charging," in *Conf. Rec. IEEE IAS Annu. Meeting*, 1996, pp. 541–548.
[13] K. J. Astrom and T. Hagglund, *PID Controllers: Theory, Design and Tuning*. Research Triangle Park, NC: ISA, 1995.
[14] A. Miller, E. Muljadi, and D. Zinger, "A variable speed wind turbine power control," *IEEE Trans. Energy Convers.*, vol. 12, no. 2, pp. 181–186, Jun. 1997.

Md. Enamul Haque (SM'97–M'03) was born in Bangladesh in 1970. He received the B.S. degree in electrical and electronic engineering from the Rajshahi University of Engineering Technology (formerly, Bangladesh Institute of Technology), Rajshahi, Bangladesh, in 1995, the M.Engg. degree in electrical engineering from the University Technology Malaysia, Skudai, Malaysia, in 1998, and the Ph.D. degree in electrical engineering from the University of New South Wales, Sydney, Australia, in 2002.

He was an Assistant Professor at King Saud University, Riyadh, Saudi Arabia, and at the United Arab Emirates University, Al-Ain, United Arab Emirates, for four years. He is currently a Lecturer in power engineering in the School of Engineering, University of Tasmania, Hobart, Australia. His research interests include distributed and renewable power generation, microgrid systems with hybrid wind/solar/fuel cell systems, power electronic applications in power systems, and DSP-based variable-speed wind-turbine generator/motor drives.

Michael Negnevitsky (M'95–SM'07) received the B.S.E.E. (Hons.) and Ph.D. degrees from the Byelorussian University of Technology, Minsk, Belarus, in 1978 and 1983, respectively.

From 1984 to 1991, he was a Senior Research Fellow and Senior Lecturer in the Department of Electrical Engineering, Byelorussian University of Technology. After arriving in Australia, he was at Monash University, Melbourne, Australia. He is currently at the University of Tasmania, Hobart, Australia, as a Chair Professor in power engineering and computational intelligence and Director of the Center for Renewable Energy and Power Systems. His interests are power system analysis, power quality, and intelligent systems applications in power systems.

Dr. Negnevitsky is a Chartered Professional Engineer and a Fellow of the Institution of Engineers Australia. He is also a member of CIGRE AP C4 (System Technical Performance) and CIGRE AP C6 (Distribution Systems and Dispersed Generation), Australian Technical Committees, and CIGRE Working Group JWG C1/C2/C6.18 (Coping with Limits for Very High Penetrations of Renewable Energy) International Technical Committee.

Kashem M. Muttaqi (A'00–SM'05) received the Ph.D. degree from Multimedia University, Cyberjaya, Malaysia, in 2001.

He was with Multimedia University as a Lecturer for three years.He was associated with the School of Engineering, University of Tasmania, Hobart, Australia, as a Lecturer/Senior Lecturer from 2003 to 2007, and with the Queensland University of Technology, Brisbane, Australia, as a Postdoctoral Research Fellow from 2000 to 2002. He is currently an Associate Professor in the School of Electrical, Computer and Telecommunications Engineering, University of Wollongong, Wollongong, Australia. He is a Member of the Integral Energy Power Quality and Reliability Center. His special fields of interests include distributed generation, renewable energy, distribution-system automation, power-system planning, intelligent grid, power quality, and reliability.